5. CONCLUSIONS

Our laboratory experiments have identified three distinct mechanisms of wave generation from finite-amplitude topography of different shapes. For smooth, sinusoidal hills, our results for waves generated by topographic excitation show that even for hills with $H/\lambda = 0.1$, the predictions of linear theory overestimate wave amplitude, although agreement is much better than for hills with $H/\lambda = 0.2$. This implies that care be taken when applying results from linear theory to such cases, for example to waves generated in the lee of the Rocky Mountains Ranges.

For large-amplitude topographies, waves are not only generated by topographic excitation but also by two non-linear mechanisms: flow over boundary-trapped lee waves and vigorous turbulence. For $\mathrm{Fr}_h < 1$, internal waves generated over and in the lee of topography match in frequency but not in amplitude, where the lee-generated amplitudes are noticeably higher. For $\mathrm{Fr}_h > 1$, the frequency and amplitude maintain constant values. The vigorous turbulence established far in the lee of the steeper triangular and rectangular hills generates smaller-scale waves of higher frequency but similar amplitude relative to the horizontal wavelength.

Acknowledgements

This research was supported by the Canadian Foundation for Climate and Atmospheric Science (CFCAS).

References

Aguilar, D. A., B. R. Sutherland, and D. J. Muraki (2005). Generation of internal waves over sinusoidal topography. *Deep Sea Res.*, submitted.

Baines, P. G. and K. P. Hoinka (1985). Stratified flow over two-dimensional topography in fluid of infinite depth: A laboratory simulation. *J. Atmos. Sci. 42*, 1614–1630.

Dalziel, S. B., G. O. Hughes, and B. R. Sutherland (2000). Whole field density measurements. *Expt. Fluids 28*, 322–335.

Dohan, K. and B. R. Sutherland (2003). Internal waves generated from a turbulent mixed region. *Phys. Fluids 15*, 488–498.

Garabato, A. C. N., K. L. Polzin, B. A. King, K. J. Heywood, and M. Visbeck (2004). Widespread intense turbulent mixing in the southern ocean. *Science 303*(5655), 210–213.

Klymak, J. M. and M. C. Gregg (2004). Tidally generated turbulence over the knight inlet sill. *J. Phys. Ocean. 34*(5), 1135–1151.

Laurent, L. S., S. Stringer, C. Garrett, and D. Perrault-Joncas (2003). The generation of internal tides at abrupt topography. *Deep Sea Res. 50*(8), 987–1003.

Ledwell, J. R., E. T. Montgomery, K. L. Polzin, L. C. S. Laurent, R. W. Schmitt, and J. M. Toole (2000). Evidence of enhanced mixing over rough topography in the abyssal ocean. *Nature 403*, 179–182.

New, A. L. and J. C. B. DaSilva (2002). Remote-sensing evidence for the local generation of internal soliton packets in the central bay of biscay. *Deep Sea Res. 49*(5), 915–934.

Rudnick, D. L., T. J. Boyd, R. E. Brainard, G. S. Carter, G. D. Egbert, M. C. Gregg, P. E. Holloway, J. M. Klymak, E. Kunze, C. M. Lee, M. D. Levine, D. S. Luther, J. P. Martin, M. A. Merrifield, J. N. Moum, J. D. Nash, R. Pinkel, L. Rainville, and T. B. Sanford (2003). From tides to mixing along the hawaiian ridge. *Science 301*(5631), 355–357.

Sutherland, B. R. (2002). Large-amplitude internal wave generation in the lee of step-shaped topography. *Geophys. Res. Lett. 29*(16). doi:10.1029/2002GL015321.

(a) Internal wave frequencies

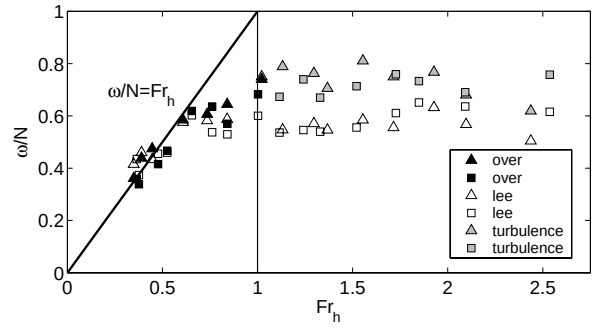

(b) Internal wave amplitudes

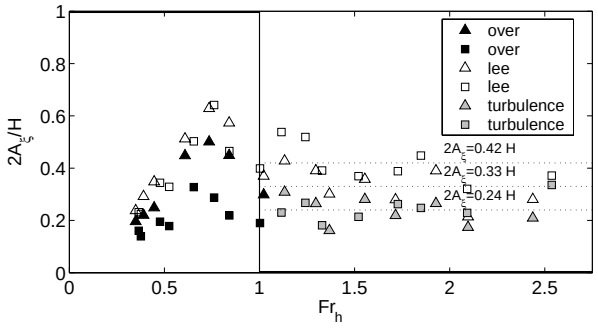

Figure 5: Plot of relative internal wave (a) frequency and (b) amplitude as a function of Fr_h measured in experiments using triangular (triangles) and rectangular (squares) topography with $H/\lambda = 0.2$ and U ranging from 0.8 - 5.2 cm/s.

shape, triangular versus rectangular, on the frequency of waves generated by the three mechanisms discussed in Section 3. For $\mathrm{Fr}_h < 1$, the results are similar to those of Figure 4a with even greater departure occuring for $0.6 < \mathrm{Fr}_h < 1$ as should be expected from such steep large-amplitude topography. More interesting results are revealed when $\mathrm{Fr}_h \gtrsim 1$. Like the large-amplitude sinusoidal hills, the waves generated in the lee have a relatively constant frequency, $\omega/N \approx 0.57 \pm 0.05$, suggesting that topographic shape does not significantly affect the structure of the boundary-trapped lee wave and resulting internal waves. This is also the case for waves generated from vigorous turbulence far in the lee. Here, the waves are higher frequency with $\omega/N \approx 0.73 \pm 0.05$, in the same range observed by Dohan and Sutherland (2003).

Figure 5b compares the relative amplitudes of the waves. For $\mathrm{Fr}_h < 1$, topographic shape is important. The amplitudes of the waves generated over the rectangular hills is significantly lower because flow separation occurs almost immediately, before the fluid can travel into the valley. The wave amplitudes in the lee appear independent of shape across all Fr_h and are similar to those generated from the sinusoidal hills. The turbulence-generated waves have relative amplitudes lower than those generated in the lee, however, when normalized by horizontal wavelength, the amplitudes are almost equal. Figure 6 illustrates this by plotting the normalized amplitude as a function of the propagation angle, $\Theta = \cos^{-1}(\omega/N)$, for the lee- and turbulence-generated waves. The plot shows that waves generated by these dynamic mechanisms propagate at preferred angles to the vertical and have large amplitudes in the sense that the amplitudes are approximately 2% of the horizontal wavelengths and 20% of the breaking amplitude.

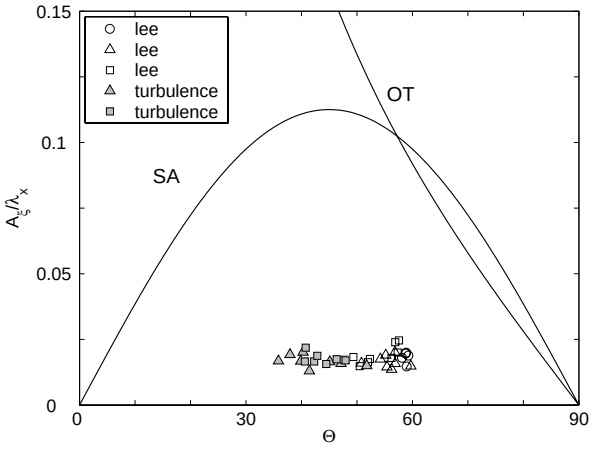

Figure 6: Plot of internal wave amplitude normalized by horizontal wavelength, A_ξ/λ_x, as a function of the propagation angle, Θ. The curve "SA" is the critical relative amplitude at which the waves should become unstable by self-acceleration. The curve "OT" is the relative amplitude at which the waves should overturn.

clearly observed at all Fr_h using the large-amplitude hills, yet only at $\mathrm{Fr}_h \gtrsim 1$ for the small-amplitude sinusoidal hills.

In Figure 3b is a wave field produced using the rectangular hills at a very fast tow speed with $\mathrm{Fr}_h > 1$. Three distinct types of waves are present. Direcly above the hills ($t = 0 - 10$ s) are high-frequency evanescent waves. In the lee of the last hill ($t = 10 - 25$ s) are lower-frequency lee waves produced by flow over a clearly visible, turbulent boundary-trapped lee wave. Far in the lee ($t = 28 - 38$ s) a vigorous turbulent region develops and results in the excitation of smaller-scale, higher-frequency waves, similar to those observed in the mixing box experiments of Dohan and Sutherland (2003). This vigorous turbulence is observed at $\mathrm{Fr}_h \gtrsim 1$ for both the steep triangular and rectangular hills.

4. QUANTITATIVE ANALYSIS

The effect of hill height on internal wave frequency and amplitude is presented in Figure 4 for the sinusoidal topography. Figure 4a plots the relative frequency of internal waves generated over (solid markers) and in the lee (open markers) of the hills. In the propagating regime ($\mathrm{Fr}_h < 1$), the observed relative frequency of vertically-propagating waves, ω/N, agrees well with the linear theory prediction, Fr_h, with significant departure occurring for $0.6 < \mathrm{Fr}_h < 1$. In this regime, the frequency of the lee waves matches that of the topographically-generated waves. In the evanescent regime ($\mathrm{Fr}_h > 1$), the frequency of the waves generated by flow over turbulent lee waves is an approximately constant function of N, in particular, $\omega/N \approx 0.51 \pm 0.02$. It is remarkable that the frequency remains constant in the presense of increasing turbulence. This frequency is observed to couple with that of the boundary-trapped lee waves, which is also found to be a constant fraction of N.

In terms of amplitude, Fig 4b shows that in the propagating regime, the relative amplitude of the waves generated over the small hills is significantly greater than that of the large

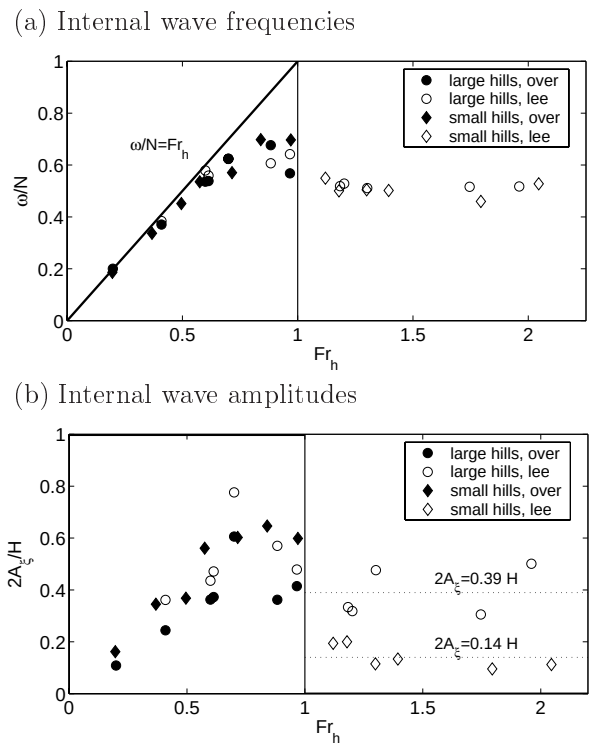

Figure 4: Plot of relative internal wave (a) frequency and (b) amplitude as a function of $\mathrm{Fr}_h = \frac{U}{N}\frac{2\pi}{\lambda}$ measured in experiments using sinusoidal topography with $H/\lambda = 0.1$ (diamonds) and 0.2 (circles) and U ranging from 0.9 - 4.9 cm/s.

hills, reaching a maximum relative amplitude of $A_\xi/H \approx 0.65 \pm 0.06$. This is consistent with linear theory, which predicts that as the hill amplitude becomes infinitesimally small, the wave amplitude approaches the hill amplitude. When H is doubled, the non-linear process of boundary-layer separation begins to dominate. This process causes fluid to separate from the hills, creating a stagnant region in the valleys and thus reducing the vertical distance displaced by the moving fluid (see Figure 3a). In the evanescent regime, the lee-generated waves maintain large amplitudes for the large hills, whereas the amplitudes drop significantly for the small hills, again consistent with the linear theory prediction that $A_\xi \to 0$ as $H \to 0$ in this regime.

Figure 5a shows the effect of topographic

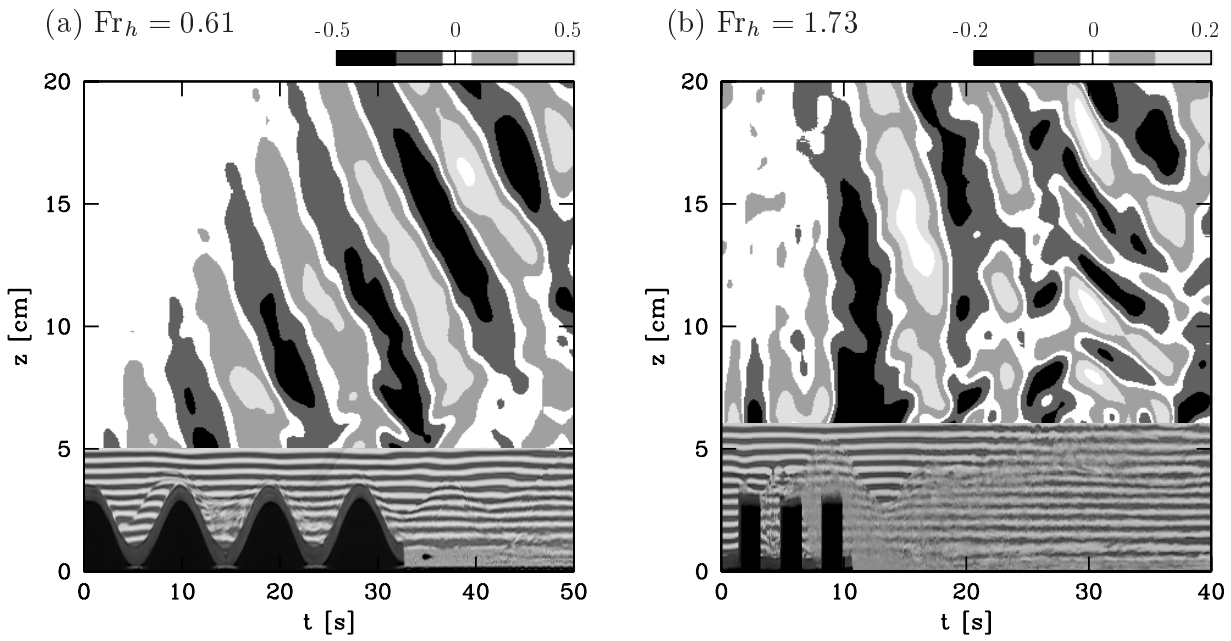

Figure 3: Vertical time series of N_t^2 [s^{-3}] for (a) large sinusoidal hills with Fr$_h$ = 0.61 and (b) rectangular hills with Fr$_h$ = 1.73. Vertical time series of raw images are superimposed to help visualize the vertically-propagating internal waves relative to the topography and boundary-trapped lee waves.

technique.

3. QUALITATIVE OBSERVATIONS

We plot contours of N_t^2 in space and time to visualize internal waves generated by three distinct mechanisms: 1) linear topographic forcing, 2) flow over boundary-trapped lee waves, and 3) turbulence. The vertical time series images are taken at a horizontal location corresponding to the initial position of the first hill, thus capturing the movement of the remaining three hills through this location.

For conceptual convenience in imagining flow over bottom topography, the images have been flipped vertically and the z-axis has been rescaled such that $z = 0$ corresponds to the bottom of the topography. Because the density difference between the salt water at the top and bottom of the tank is small compared to the density of the water itself, the fluid is Boussinesq. Hence there is no dynamic difference between waves propagating downward from topography towed along the surface of the fluid and waves propagating upward from topography towed along the bottom of the tank. The vertical time series image of the horizontal lines is superimposed at the bottom of the frame to reveal flow structures in the lee of topography and so illustrate the relationships between the excitation mechanisms and the resulting wave fields.

Figure 3a shows a wave field produced from an experiment using the large-amplitude sinusoidal hills with Fr$_h$ < 1. The regular wave pattern directly above the hills is the result of fluid flowing in and out of the hill valleys, a mechanism commonly referred to as topographic forcing. In the lee of the topography, the wave field persists and the amplitude increases. These waves are generated when fluid flows over a hump-shaped disturbance in the lee of topography, called a boundary-trapped lee wave, similar to that observed downstream of a single "Witch of Agnesi" hill (Baines and Hoinka, 1985) and downstream of a smooth step (Sutherland, 2002). Such a feature is

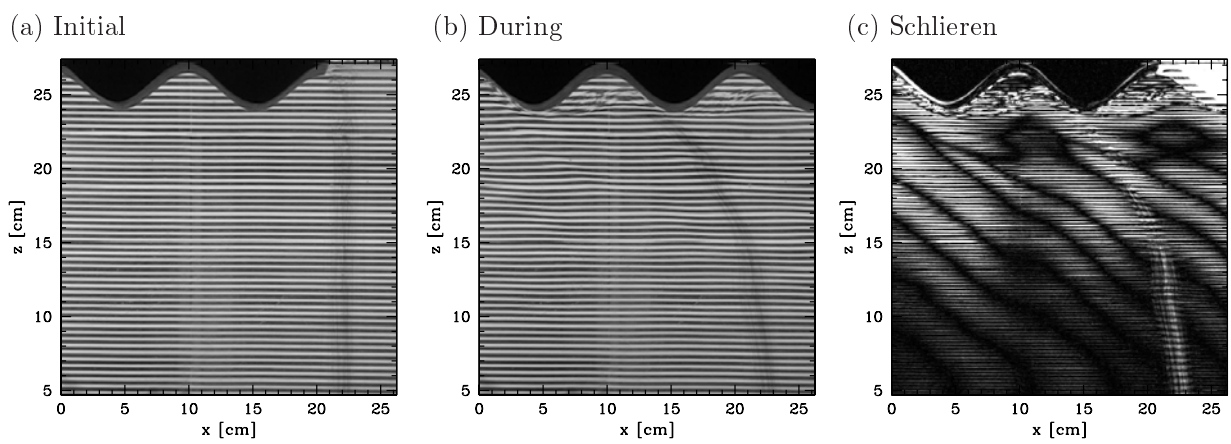

Figure 2: (a) Snapshot image taken before the start of an experiment using large sinusoidal hills with parameters, $H/\lambda = 0.2$ cm and $\mathrm{Fr}_h = 0.41$. The wave field is revealed by subtracting the image in (a) from the image taken during the experiment in (b), yielding the synthetic schlieren image in (c).

Four model topographies were studied: small- and large-amplitude sinusoidal hills with peak-to-peak heights, $H = 1.3$ cm and 2.6 cm respectively, as well as triangular and rectangular hills with $H = 2.6$ cm. The topographies spanned four hill wavelenghts with $\lambda = 13.7$ cm. Non-dimensionally, the relative height to separation distances were $H/\lambda = 0.1$ and 0.2 for the small- and large-amplitude hills respectively. Thus, the small hills are comparable in relative size to the Rocky Mountain Ranges.

Model topographies were towed from left to right at approximately constant speeds ranging from $U = 0.8 - 5.2$ cm/s with corresponding Froude numbers, $\mathrm{Fr}_h = 0.2 - 2.5$. Viewed in a frame of reference moving with the topography, the experiment models the generation of internal waves due to a constant flow over the hills. As Fr_h increased, the flow between and in the lee of the hills underwent a transition to turbulence, which altered the generation of waves from direct topographic generation to indirect dynamic generation in the lee.

The waves themselves were visualized and their characteristics measured using a non-obtrusive optical technique called "synthetic schlieren" (Dalziel et al., 2000). The experiment was set up with a digital camera focused on a screen of illuminated horizontal black and white lines positioned behind the tank (see Figure 1b). When waves move within the tank, they stretch and compress isopycnal surfaces, thereby changing the local density gradient. This consequently changes the index of refraction of light through the medium, thus altering the image of horizontal lines. The schlieren technique records the distortion of the image of horizontal lines as compared to an initial image. Figure 2 illustrates this technique by comparing three images: a snapshot taken before the start of an experiment, a snapshot taken during the experiment, and the schlieren image obtained by taking the difference between the two. The schlieren image clearly reveals the wave field below the hills.

The amplitude of vertical dispacement of the waves, A_ξ, can be determined from $A_{N_t^2}$ using the Boussinesq relation for linear plane waves in a uniformly stratified fluid,

$$\begin{aligned} A_{N_t^2} &= k_x N^3 \sin\Theta A_\xi, \\ &= 2\pi N^3 \sqrt{1 - \mathrm{Fr}_h{}^2}\, \frac{A_\xi}{\lambda_x} \end{aligned} \tag{2}$$

where k_x and λ_x are the horizontal wavenumber and wavelength respectively, Θ is the angle of wave propagation to the vertical, and $N_t^2 = \frac{\partial}{\partial t} N^2$ is determined from the schlieren

J6.7 LABORATORY GENERATION OF INTERNAL WAVES FROM ROUGH TOPOGRAPHY

Dawn A. Aguilar*, and B. R. Sutherland
University of Alberta, Edmonton, Canada

1. INTRODUCTION

Recent observations in the deep-ocean have shown that internal waves are generated most significantly by the flow of tides over the rough terrain of the ocean floor, such as sea mounts, ridges, and canyons (New and DaSilva, 2002; Rudnick et al., 2003; Laurent et al., 2003). In many of these sites, energetic turbulence has been observed (Ledwell et al., 2000; Klymak and Gregg, 2004; Garabato et al., 2004) and presumably results directly as a consequence of flow over topography and wave breaking.

The mechanisms by which internal waves are generated from topography are poorly understood beyond the suppositions of linear and inviscid theories, which do not take into account the dynamics of boundary layer separation. Linear theory restricts predictions of topographically-generated waves to those launched by smooth hills with small aspect ratios of the topographic height, H, to width, L. In such cases, theory predicts that propagating waves will be generated when the non-dimensional Froude number, $\mathrm{Fr}_h < 1$. Otherwise, the waves will be "evanescent" meaning that the amplitude will decay exponentially. Here, Fr_h is defined in terms of the flow speed, U, the buoyancy frequency, N, and the topographic width, L, by

$$\mathrm{Fr}_h \equiv \frac{U}{N}\frac{2\pi}{L}, \qquad (1)$$

where N is defined in terms of the background density, $\overline{\rho}$, a characteristic density, ρ_0, and the acceleration due to gravity, g, by $N^2 = -(g/\rho_0)d\overline{\rho}/dz$.

* *Corresponding author address*: Dept. Mathematical and Statistical Sciences, Univ. Alberta, Edmonton, AB, Canada T6G 2G1; e-mail: dawn.aguilar@ualberta.ca.

The present research uses laboratory experiments to investigate the ways in which waves are generated by flow over and in the lee of finite-amplitude topography. Beginning with smooth sinuosoidal hills of different hill amplitudes, the limitations of linear theory are explored (see also Aguilar et al., 2005). Non-smooth, large-amplitude topographies are used to further examine the effects of shape and flow speed on wave generation.

2. EXPERIMENTAL SET-UP

Experiments were performed in a glass tank with dimensions 197 cm long by 50 cm high by 17.5 cm wide as shown in Figure 1a. The tank was filled with uniformly salt-stratified water to achieve a constant buoyancy frequency of $N = 1.09 \pm 0.03$ s^{-1}.

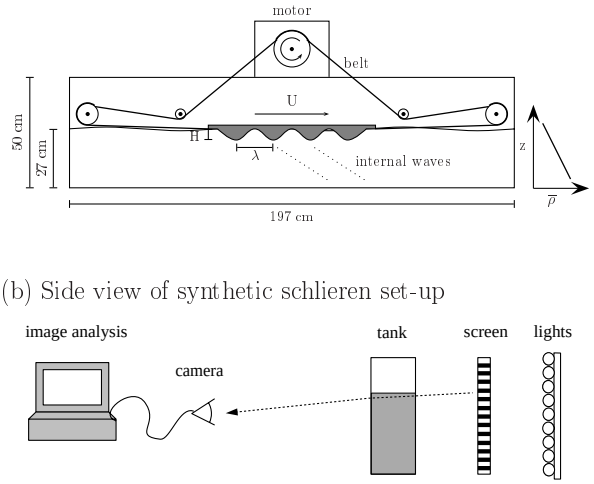

Figure 1: (a) Front view schematic of tank and towing apparatus used to generate vertically propagating internal waves and (b) side view schematic of synthetic schlieren set-up used to visualize and measure wave properties.